FACTORS CONTROLLING THE SIZE DISTRIBUTIONS OF LUNAR PYROCLASTS. Cerith R. Morgan[1], Lionel Wilson[1,2] and James W. Head[2]. [1]Lancaster Environment Centre, Lancaster University, Lancaster LA1 4YQ, U.K. [2]Department of Earth, Environmental and Planetary Sciences, Brown University, Providence, RI 02912 USA (cerithrhys@hotmail.com; l.wilson@lancaster.ac.uk; james_head@brown.edu)

Introduction: Spectroscopic data [e.g., 1] show pyroclastic deposits from explosive eruptions to be widespread on the nearside of the Moon, with a wide range of lateral extents. However, our only data on pyroclast grain size distributions come from the glass beads sampled by the Apollo missions [e.g., 2]. Here we discuss the relative importance of the factors that influence pyroclast size distributions. In a companion abstract [3] we use these results to find the ranges of magma volatile contents and discharge rates required to produce the observed spectrum of lunar pyroclastic deposits.

Background: Physical models of steady explosive volcanic eruptions in the lunar vacuum [4] show that the distances to which pyroclasts can be ejected depend on the mass fraction of volatiles of a given molecular mass released from the magma and on the pyroclast size distribution. The generally sub-mm sizes (Fig. 1) of the sampled lunar pyroclastic glass beads [2] are qualitatively consistent with the expected extreme fragmentation of lunar magmas as they erupt into a vacuum [5], but the distances between sample sites and their respective vents are unknown and we have probably not sampled the coarsest parts of the pyroclast size distributions.

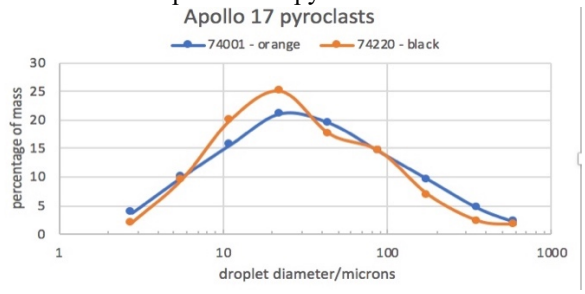

Figure 1. Mass distributions in Apollo 17 pyroclasts.

The efficiency with which a pyroclast is accelerated by expanding gases in a volcanic explosion is a function of the clast size. The vertical velocities of all clasts lag behind the vertical component of the local gas speed by the terminal velocities of the clasts in the gas [6]. Loss of coarse clasts near the vent, where the pressure in the expanding gas is still high, increases the effective gas mass fraction in the remaining gas-particle mixture so that small clasts reach greater velocities than if the size distribution were monodisperse [4]. Thus a range of clast sizes is expected at any given distance from the vent (as seen in the Apollo samples), but interpretation of these sample size distributions requires a prediction of the likely total clast size distribution generated by magma fragmentation in the vent. We attempt that here.

Analysis: [7] describe the volatile release pattern in ascending picritic lunar magmas. CO is generated in amounts up to ~1300 ppm, >90% at depths > ~50 km, ~10% between ~50 and ~0.5 km, and none shallower than 0.5 km. In contrast >98% of the up to ~850 ppm of water is released progressively at depths < ~500 m. S-compounds and halogens also exsolve, but we use water as a proxy for all late-stage volatiles and calculate the volume fractions occupied by CO and H_2O gas bubbles, and their sizes, as a function of depth.

The initial size of gas bubbles nucleating in magmas depends on availability of nuclei, e.g. phenocrysts, degree of supersaturation, surface tension of the gas-liquid interface, and decompression rate [8]; sizes of order 5 microns seem likely [9]. Bubbles grow by decompression, diffusion of additional volatiles from the liquid, coalescence due to collisions in sheared flow, and Ostwald ripening. With lunar CO released at great depths, growth is mainly by decompression and collision. Water is released while rising ~ 500 m over a time span of order 50 s [4] so supersaturation-driven bubble nucleation is also very important [8]. If gas is released continuously between nucleation and fragmentation, the cumulative bubble size distribution is $N/N_0 = \exp[-\phi/(G\,t)]$ where N is the total number per unit volume of bubbles of diameter ϕ and smaller, t is the magma ascent time scale and G is the bubble radius growth rate [8]. The relative number of bubbles of different sizes is $n(\phi) = dN(\phi)/d\phi$. The bubble growth rates found by various authors differ dramatically, from ~3×10^{-9} m/s for 10 ppm water in basalt [9: decompression laboratory experiment] through ~6×10^{-8} m/s for CO_2 in basalts [10: inference from samples, slow magma rise speeds] to 10^{-5} m/s for ~10000 ppm water in basalt [8: inference from samples, high magma rise speeds]. Since the distances between bubbles in magmas must be proportional to the density of nucleation sites, and greater magma rise speeds favor supersaturation and high densities, we prefer growth rates comparable to those from [8] for lunar water release, but scale them by the total water content, using $G = 5.46 \times 10^{-7}$ m s^{-1}. We infer that smaller rates apply to CO, and using the same rationale estimate $G = 1.8 \times 10^{-7}$ m s^{-1}. We assume that as bubbles collapse during magma fragmentation they produce magma droplets, the eventual pyroclasts, with diameters comparable to those of the bubbles - the ratio would be 0.97 for perfect cubic packing. We then multiply the number distribution of pyroclasts by the volume of each size class and, since all of the droplets have essentially the same density, this

yields the mass distribution for comparison with the lunar data in Fig. 1. Using the above bubble growth parameters we find the very bimodal pyroclast mass distributions for droplets shown in Fig. 2.

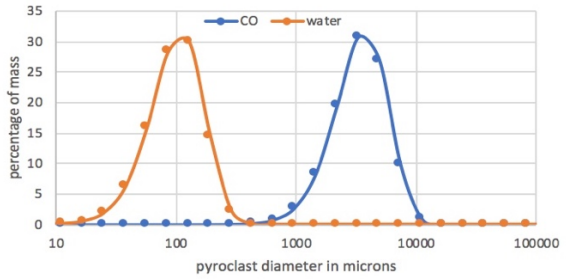

Figure 2. Typical predicted CO and H_2O pyroclast size distribution in steadily erupting lunar magma.

The above superposition of two pyroclast size distributions is inevitably an approximation. The actual size distribution produced by a fragmenting magma is related to the bubble size distribution via the bubble packing, determined by both the size distribution and total vesicularity. We are currently exploring the use of a model developed for metal foams [11] involving inversion geometry to determine the liquid volumes between bubbles by defining a network of struts and nodes. The nodes become the pyroclasts after fragmentation, as shown in Fig. 3 for >90% vesicular hawaiian reticulite.

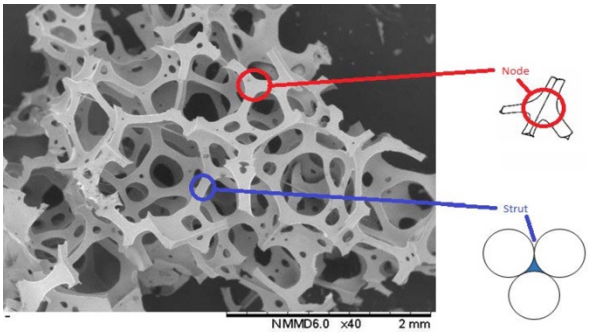

Figure 3. Strut and node structure in vesicular reticulite. Image courtesy of Cardiff Catalysis Institute.

Pyroclasts accelerated by expanding gases quickly attain the horizontal component of the gas speed but lag the vertical gas speed component by their terminal velocity. We evaluate the terminal velocities of the various particle size classes, applying the Cunningham correction for the change in gas-particle drag force as the gas density decreases and the Knudsen number, Kn, becomes > 1 [12]. When Kn is >> 1 for a given clast size drag becomes negligible and clasts continue on ballistic trajectories. Large clasts fall out of the expanding gas-particle mixture quickly. The remaining clasts see an effectively increased gas mass fraction and travel to greater distances than if no large clasts were present [4].

The lower end of the pyroclast size range is fixed by the size of nuceating bubbles, ~20 μm. Large diameter clasts are most likely to form when bubble coalescence or Ostwald ripening occur, converting a large number of small bubbles to a small number of large bubbles. Both mechanisms are encouraged by slow magma rise speed [4], and so it is towards end of an eruption, when the magma rise speed is decreasing [13], that polarization into coarse near-vent and fine-grained far-field deposits is likely to occur. The extreme version of this is strombolian activity, with most of the CO bubbles coalescing into slugs that almost fill the conduit and reach the surface intermittently. The magma between slugs releases its H_2O and fragments into droplets that are then accelerated by both the expanding H_2O vapor and the CO, leading to at least a doubling of the effective gas content of the mixture. The largest dark mantle deposits on the Moon can likely be explained by this process as we consider in our companion abstract [3].

A final issue concerns the possibility of break-up of molten pyroclasts as a result of hydrodynamic instabilities induced by their velocity U relative to the gas. Break-up under shearing forces is controlled by three dimensionless numbers [14], the Reynolds number, $Re = (\rho_g D U)/\mu_g$, the Weber number $We = (\rho_g U^2 D)/\sigma$, and the Ohnesorge number, $Oh = \mu_g/(\rho_l D \sigma)^{1/2}$, where ρ_g and μ_g are the density and viscosity of the gas, ρ_l is the density of the liquid, σ is the surface tension of the liquid-gas interface, and D is again the diameter of the clast. Inserting typical values we find that break-up is unlikely to be important for droplets smaller than ~10 mm but would quickly become very important for droplets larger than ~20 mm, perhaps explaining their absence from Apollo samples.

References: [1] Jawin E. R. et al. (2015) *JGR-Planets, 120*, 1310–1331. [2] Heiken G. H. et al. (1974) *GCA, 38*, 1703–1718. [3] Wilson L., Head J.W. and Morgan C. This meeting. [4] Wilson L. & Head, J.W. (2017) *Icarus, 283*, 146–175. [5] Wilson L. & Head J. W. (1981) *JGR, 86*, 2971–3001. [6] Wilson L. (1999) *Geophys.J.Int., 136*, 609–619. [7] Rutherford M. J. et al. (2017) *Amer. Min., 102*, 2045–2053. [8] Mangan M. T. & Cashman K. V. (1996) *JVGR, 73*, 1–18. [9] Masotta M. et al. (2014) *Contrib. Min. Petrol. 167*, 976, 14 pp.[10] Sarda P. & Graham D. (1990) *EPSL, 97*, 268–289. [11] Smorygo O. et al. (2011) *Acta Materiala, 59*, 2669–2678. [12] Knudsen M & Weber S. (1911) *Annalen der Physik, 341*, 981-994. [13] Wilson L. & Head, J.W. (2018) *GRL, 45*, 5852–5859. [14] Jain M. et al. (2018) *Proc. Royal Soc. A471*, 20130930.